SIN-CHN SCIENTIFIC PRESS PTE.LTD.

Molecular & Cellular Biomechanics 2025, 22(4), 1586.
https://doi.org/10.62617/mcb1586

Article

Influence of SSM-based skiing biomechanical analysis on tourist travel experience

Nian Liu[1], Runchu Fu[2,*], Tianchi Fu[2]

[1] Department of Convergence Management, Corporate Management Major, Woosong University, Daejeon 34606, South Korea
[2] Woosong University, Daejeon 34606, South Korea
*** Corresponding author:** Runchu Fu, a-biaofu@hotmail.com

CITATION

Liu N, Fu R, Fu T. Influence of SSM-based skiing biomechanical analysis on tourist travel experience. Molecular & Cellular Biomechanics. 2025; 22(4): 1586. https://doi.org/10.62617/mcb1586

ARTICLE INFO

Received: 17 February 2025
Accepted: 6 March 2025
Available online: 12 March 2025

Abstract: Skiing, as a popular winter sport, attracts a large number of tourists to ski resorts for an immersive experience. To improve tourists' travel experience and ensure their safety, this study proposes a skiing biomechanical analysis method based on the Statistical Shape Model. The study conducts 3D reverse modeling of tourists' ankle joints and constructs mechanical models for the talus and calcaneus. Finally, the model is used to analyze the impact of ankle joint morphology on the axis of rotation. Experimental results show that among the three indicators in the evaluation of the Statistical Shape Model, the compactness of the talus increases from 29,800 to 41,500, and the calcaneus increases from 39,800 to 64,700. The generalization value of the talus decreases from 97,800 to 93,400, and the calcaneus decreases from 116,900 to 111,500. After the statistical shape model of the improved skiing equipment, the tourist experience satisfaction is more than 85%. The results indicate that the morphology of the talus and calcaneus significantly affects the axis of rotation. By analyzing the biomechanics of tourists' ankle joints during skiing, a deeper understanding of the mechanical characteristics in skiing is obtained, providing a theoretical basis for optimizing tourists' travel experience. The morphological features of the ankle joint directly impact tourists' balance and stability during skiing, thereby influencing both the safety and enjoyment of the sport.

Keywords: statistical shape model; skiing; biomechanical analysis; tourism experience; ankle joint

1. Introduction

Skiing biomechanics includes force analysis and movement states of skiing, where the movement states involve tourists' adjustment of force techniques during skiing. Therefore, the sensory feedback from the ankle joint during movement is crucial to the tourism experience of the tourists [1,2]. The human ankle joint, as an important component of bone biomechanics, tightly connects the bones, muscles, and ligaments, driving the lower limbs for gait movement [3]. Once injured, the human ankle joint can lead to neuromuscular impairments, resulting in a decline in motor function. As a result, many scholars have conducted research on ankle joint movement. For example, Reynolds R F et al. studied the relationship between ankle joint stiffness and calf muscle motion during standing to address issues such as instability in calf muscle control due to tendon compliance. The results showed that the natural changes in ankle joint stiffness altered the degree of abnormal calf muscle motion during standing [4]. Li et al. investigated the differences in cortical activation during dorsiflexion and plantarflexion between patients with chronic ankle instability and healthy individuals, designing an open-close cycle for movement and rest periods [5]. These studies indicate that research on ankle joint biomechanics can help explain the

instability factors related to ankle injuries. However, since the human body is often in a walking or exercising state, the joints are continuously subject to biomechanical changes. Therefore, a better coordination system for three-dimensional simulation is needed [6–8]. A three-dimensional simulation system can analyze the interrelation of ankle joint movements between individuals and provide data-driven analysis and visual 3D presentation. As a result, many scholars have conducted research on the Statistical Shape Model (SSM). Trentadue et al. proposed a multi-domain statistical shape modeling method to quantify joint morphology at high speed. The results showed that the method captured 76.2% of the morphological changes in the first five variance models [9]. In summary, there is considerable research on SSM and the ankle joint, but studies combining both are limited. Therefore, to gain a more detailed understanding of ankle joint movement and improve the tourist experience, this study proposes a skiing biomechanical analysis method based on SSM. This method innovatively optimizes data collection by using optical motion capture systems and 3D reverse modeling, aiming to provide mechanical theoretical data on tourists' ankle joints in skiing areas and promote tourism safety.

2. Methods and materials

2.1. Data collection and 3D reverse modeling

When the human body engages in skiing, the lower limb joints can integrate surrounding mechanical signals to respond and adjust their own characteristics in real time [10]. However, during human movement, misalignment or injuries between bones can occur, affecting the overall skiing experience [11]. To address the challenges of data collection during lower limb joint movement, this study uses an optical motion capture system to collect kinematic data of the ankle joint. The optical motion capture system can not only extract features from the target but also infer the body's movement state through changes in continuous frame images [12,13]. The modified centroid and ankle joint center distance are expressed as shown in Equation (1).

$$L_1 = B_0 + B_1 m + B_2 h \tag{1}$$

In Equation (1), L_1 represents the centroid of the shank segment, B_0, B_1, and B_2 are the binary regression coefficients, and the specific meanings are intercept terms, distance variables between joints and joints, and human height coefficient. h indicates human height, and m represents the distance between joints. The calculation of the modified kinematic principle is expressed as shown in Equation (2).

$$\begin{cases} ds^i = p^{i+1} - p^i = \left(x^{i+1} - x^i, y^{i+1} - y^i, z^{i+1} - z^i\right) \\ u^i = \dfrac{ds^i}{dt} = \dfrac{p^{i+1} - p^i}{dt} \\ a^i = \dfrac{u^{i+1} - u^i}{dt} = \dfrac{p^{i+1} - 2p^i + p^{i-1}}{dt^2} \end{cases} \tag{2}$$

In Equation (2), dt represents the time interval, ds^i is the centroid displacement, and the center of mass displacement is a vector containing x, y, and z three-direction transformations. The average velocity and acceleration are u^i and a^i, respectively,

used to analyze the motion state of the object. Since bones, muscles, and ligaments collaborate during movement to perform any action, the optical motion capture system is used to calculate the corresponding balance of joint forces and joint moments. The balance measurement of the joint is shown in **Figure 1**.

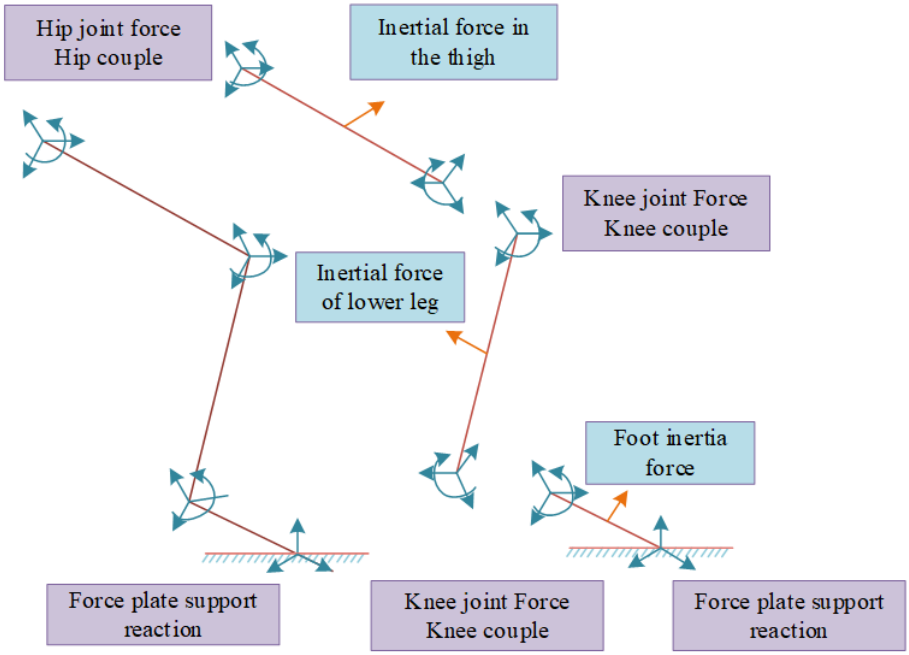

Figure 1. Schematic diagram of balance joint measurement.

As shown in **Figure 1**, in a microgravity environment, the lower limb of the human body undergoes composite rotation around the joints, with each joint acting as a different hinge. The forces acting on the lower limb are primarily divided into hip joint forces and hip joint moments, knee joint forces and knee joint moments, and ankle joint forces and ankle joint moments. The hip joint force and moment are mainly generated by the inertia of the thigh segment, the knee joint force and moment are mainly caused by the inertia of the shank segment, and the ankle joint force and moment are driven by the inertia of the foot segment. The force plate reaction force, during measurement, can measure the reaction forces of the ankle joint force and moment. The balance equation for the ankle joint force and moment is shown in Equation (3).

$$\begin{cases} \sum F = F_a + F_b + F_c = 0 \\ \sum M = F_a \times L + M_b + M_c = 0 \end{cases} \tag{3}$$

In Equation (3), F and M represent the balance of ankle joint force and moment, a is the inertial force, b is the proximal force, and c is the distal force. Equation (3) does not include the calculation of segmental gravity effects. Although the optical motion capture system can calculate joint forces and other parameters for various human joints, there are still some limitations in visual data collection. Therefore, based on the optical motion capture system, this study uses 3D reverse modeling to further analyze key elements of the human foot and ankle. 3D reverse modeling allows for

data processing and analytical reconstruction of physical objects and can reverse-engineer the required model [14,15]. The reverse modeling was performed using software such as Geomagic Design X and Creo to create a perfect polygon model and network from the scanned point cloud data and a CAD model of a surface on the multi-faceted data. The global distance mean formula for denoising point clouds in 3D reverse modeling is shown in Equation (4).

$$D = \frac{1}{N}\sum_{i=1}^{N} d_i \tag{4}$$

In Equation (4), i represents a specific point cloud, N is the total number of human joint point clouds, and d_i is the average distance between a point cloud and its neighboring points. The ankle-foot skiing orthosis designed using 3D reverse modeling and the optical motion capture system is shown in **Figure 2**.

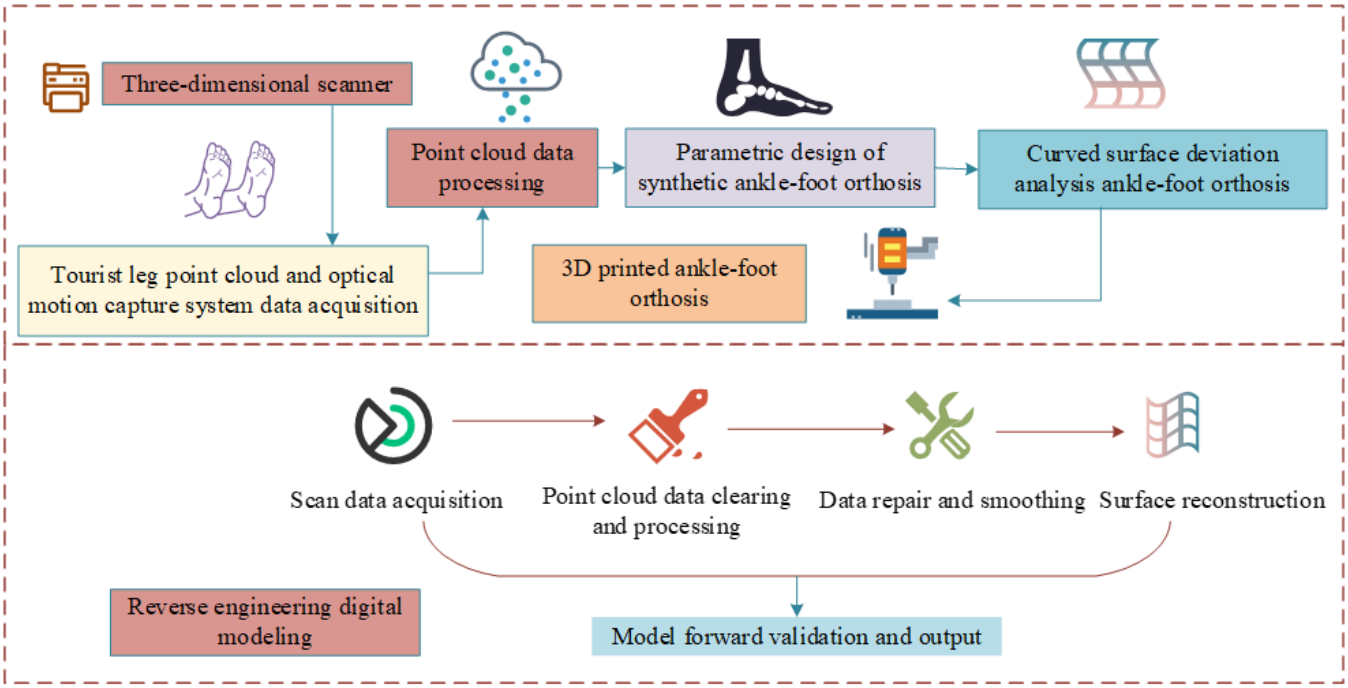

Figure 2. Ankle-foot skiing orthosis workflow diagram.

As shown in **Figure 2**, the ankle-foot digital orthosis primarily uses 3D reverse modeling and the optical motion capture system for digital design. The process begins with the use of a 3D scanner to scan the bones and joints. Then, joint data of the tourist's foot and leg are collected and processed through point clouds and the optical motion capture system. The parameterized design station generates the ankle-foot orthosis to replace traditional positive mold production. Afterward, surface deviation analysis is performed on the ankle-foot orthosis, and 3D printing technology is used to print the model. Finally, the printed model undergoes forward validation and optimization to determine whether the ankle-foot orthosis helps enhance the ankle joint's recovery ability in case of injury during skiing. The forward surface reconstruction of the model was performed using software such as Geomagic Studio and Autodesk Fusion 360 to process point cloud data and polygon networks to keep

the surface smooth and continuous. The surface fitting node vector is shown in Equation (5).

$$\begin{cases} U = [u_0, u_1, \cdots, u_{m+p}] \\ V = [v_0, v_1, \cdots, v_{n+p}] \end{cases} \tag{5}$$

In Equation (5), u and v represent the parameter axes, and U and V are the node vectors. The surface mathematical model is expressed as shown in Equation (6).

$$S(u,v) = \sum_{i=0}^{m} \sum_{j=0}^{n} N_{i,p}(u) N_{j,q}(v) P_{i,j}, u, v \in (0,1) \tag{6}$$

In Equation (6), $S(u,v)$ represents the given control vertex in the $P_{i,j}$ space points, determining the surface shape. $N_{i,p}(u)$ and $N_{j,q}(v)$ are the B-spline basis functions of the node vectors; the contribution weight of the control vertex to the surface is calculated by the parameters u and v. In summary, the study, through 3D reverse modeling and the optical motion capture system, models and analyzes ankle-foot joint data. This approach can meet the complex surface model creation requirements and can promptly identify the center of mass of tourists' bodies during skiing.

2.2. Construction of ankle joint model based on the SSM

With the development and innovation of global intelligence, ice and snow sports are gradually being popularized and promoted in the public eye [16]. However, the general public often struggles to experience the joy of skiing due to a lack of relevant theoretical guidance and cannot accurately master the skills of applying force during skiing [17]. Although 3D reverse modeling and optical motion capture systems can collect some data from the human body, they cannot accurately capture the morphological changes of the foot bones. Therefore, based on 3D reverse modeling and the optical motion capture system, this study constructs an ankle joint model based on SSM to analyze the potential impact of different talus morphologies on the ankle joint. SSM can specifically describe and analyze the shape of an object, identifying various principal component shapes, functions, and other differences [18]. The 3D coordinates generated by SSM for the ankle joint samples are shown in Equation (7).

$$U = [(x_1, y_1, z_1), (x_2, y_2, z_2), \ldots, (x_n, y_n, z_n)] \tag{7}$$

In Equation (7), U represents the total feature points of the ankle joint sample, with the sample containing n individual points. The specific process of shape matching for the ankle joint using SSM is shown in **Figure 3**.

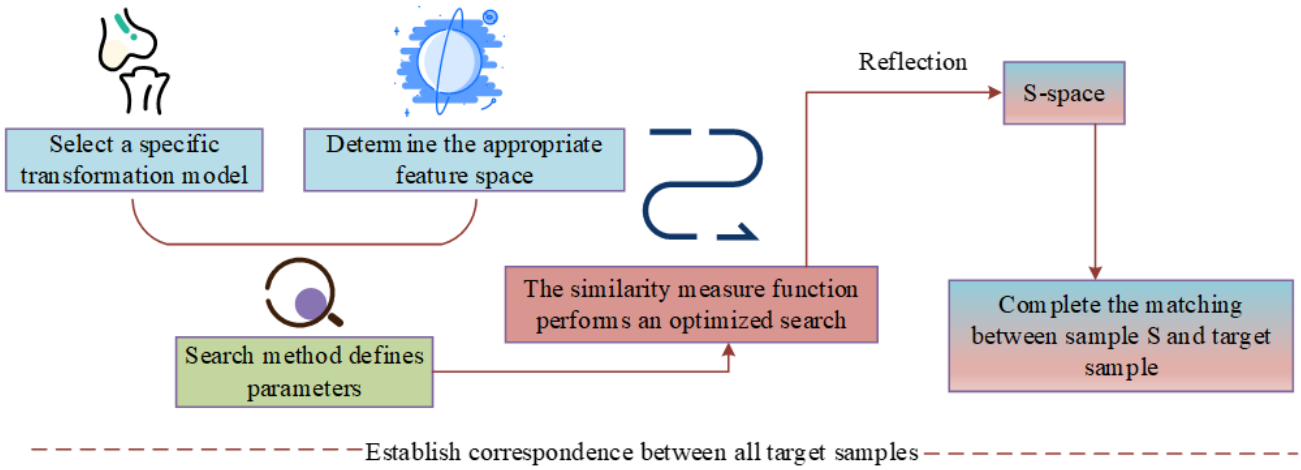

Figure 3. Schematic diagram of the shape matching process.

As shown in **Figure 3**, the shape matching of the ankle joint using SSM first requires aligning the target sample, selecting a suitable transformation model and feature space, and then setting parameters for the chosen model. A search method is used to define the possible variation intervals for the parameters. Once the variation intervals are determined, an optimization search is performed using a similarity measure function to identify the unknown parameters, with the primary search range being in two-dimensional or three-dimensional space. Finally, the selected target sample is mapped to the target sample template space S, completing the shape matching. After the matching process is completed, principal component analysis is applied to generate the SSM. The calculation of the sample's principal components is shown in Equation (8).

$$CP_i = \lambda_i P_i \tag{8}$$

In Equation (8), C represents the covariance matrix, P_i is the eigenvector, and λ_i denotes the corresponding eigenvalue. The main mode of variation can be derived from Equation (8) as shown in Equation (9).

$$U = \bar{U} + \sum_{m=1}^{M} \lambda_m P_m \tag{9}$$

In Equation (9), m represents the variation mode coefficient, $\bar{U}$ and U are the mean shape model and the SSM result, and λ_m and P_m are the corresponding eigenvalue and eigenvector. To ensure the accuracy of the data modeling when using the SSM for the ankle joint, the study applies an error correction to the axial force of the ankle joint. The specific correction algorithm process is shown in **Figure 4**.

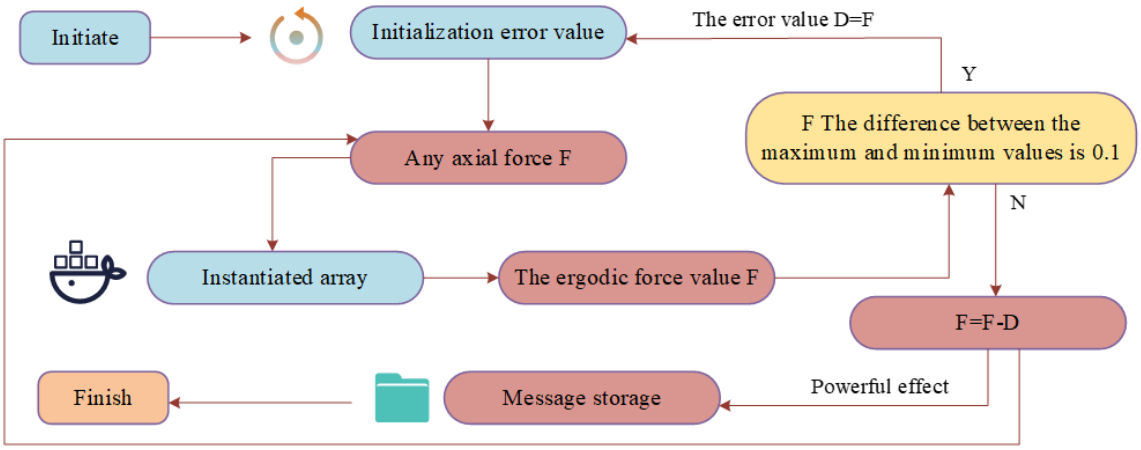

Figure 4. Correction algorithm flow chart.

As shown in **Figure 4**, when correcting errors in the ankle joint axial force data, the process first requires the initialization of the error values. Then, the axial force *F* is constructed into an instantiated array, and the axial force data is cached. The data in the cached area is then iterated and calculated to determine whether the difference between the maximum and minimum axial force values *F* exceeds 0.1 N. If the difference is greater than 0.1 N, the sensor for the data becomes active. The actual axial force value *F* is calculated by subtracting the error value D from the axial force value *F*, resulting in the accurate ankle joint axial force data. The local coordinate representation of the talus in the ankle joint is shown in Equation (10).

$$\begin{cases} x_1 = (x_0 + x_2)/2 \\ y_1 = (y_0 + y_2)/2 \\ z_1 = (z_0 + z_2)/2 \end{cases} \tag{10}$$

In Equation (10), (x_3, y_3, z_3) represents the origin of the local coordinates, (x_0, y_0, z_0) denotes the coordinates of the medial malleolus feature point, and (x_2, y_2, z_2) refers to the coordinates of the lateral malleolus. The vector x is represented as shown in Equation (11).

$$\vec{x} = (x_1 - x_3, y_1 - y_3, z_1 - z_3) \tag{11}$$

In Equation (11), x axis represents the direction from the talus origin to the talar head, and (x_3, y_3, z_3) refers to the coordinates of the talar head. In this study, Mimics software was used to scan the ankle joint and its surrounding structure in 360° and to reconstruct the 3D model. The ankle joint model based on SSM developed by the study is shown in **Figure 5**.

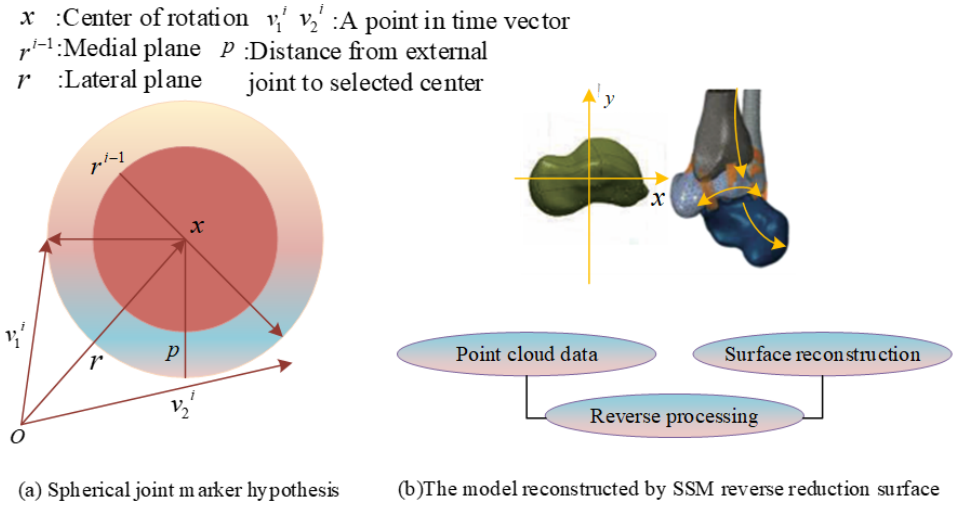

Figure 5. Schematic diagram of ankle joint model based on SSM.

From **Figure 5a**, x and n represent the spherical joint marking points, assuming the rotation center and direction vector. The center of the circle is the rotation axis, p is the distance from the external joint to the selected center, and r and r^{i-1} represent the lateral and medial planes, respectively. ${v_1}^i$ and ${v_2}^i$ represent vectors at a certain time point. From **Figure 5b**, it can be seen that the SSM-based ankle joint model requires point cloud data for data import, followed by surface reconstruction to generate a physical simulation model. The hinge joint center expression is shown in Equation (12).

$$ {x_c}^i = x + \tau^i n \tag{12}$$

In Equation (12), τ^i represents the set constant in the vector, and n is the direction vector. In summary, the ankle joint plays a crucial role in the biomechanical foot and ankle motion spatial orientation. By utilizing 3D reverse modeling and optical motion capture systems, comprehensive visual data collection of the human body can be achieved. On this basis, the proposed SSM ankle joint model allows for a more comprehensive understanding of ankle joint movement, which is beneficial for improving related sports equipment in ski areas.

3. Results

3.1. Evaluation of ankle joint model based on the SSM

To verify the performance superiority of the SSM-based ankle joint model, the study compared it with the Principal Component Analysis (PCA) ankle joint model, the Active Shape Model (ASM) ankle joint model, and the 3D Deformable Model (3D DM) ankle joint model. The experiment utilized the Tianyuan 3D motion capture system 3DMoCaP for ankle joint data collection, SolidWorks Simulation and Geomagic finite element simulation software for preprocessing, the Windows 10 operating system, and the Footscan flatfoot pressure testing system for the experiment. In order to make the experimental data fair, 50 volunteers from Peking Union Medical College Hospital were selected as the research objects of the SSM ankle joint model, and 150 tourists from Miyun Ski Resort were selected for comparison. The statistical

test showed that the age test stage of volunteers and tourists mainly ranged from 15 to 35, the skiing proficiency was intermediate, and they were able to skate on the ski slope at 10° to 25° with *P* values greater than 0.05. There were no significant differences in the distribution of age, gender, and height of the subjects. Among them, the intermediate wave track practice area of Miyun Nanshan Ski Resort is 500 m long and has an 18° slope. The sample information is shown in **Table 1**.

Table 1. Participant information data.

Sample	Age	Sex	Height	*t*	*P*	Skiing proficiency level
Volunteer	15–18	Male 5/Female 3	158–178 cm	1.2	0.08 > 0.05	Intermediate (Slope 10°–25°)
	20–25	Male 13/Female 12	160–182 cm	0.8	0.12 > 0.05	Intermediate (Slope 10°–25°)
	28–35	Male 10/Female 7	162–185 cm	1.5	0.06 > 0.05	Intermediate (Slope 10°–25°)
Visitor	15–18	Male 35/Female 25	160–178 cm	1.2	0.08 > 0.05	Intermediate (Slope 10°–25°)
	20–25	Male 15/Female 12	160–182 cm	1.3	0.09 > 0.05	Intermediate (Slope 10°–25°)
	28–35	Male 42/Female 21	162–185 cm	1.7	0.08 > 0.05	Intermediate (Slope 10°–25°)

The SSM, PCA, ASM, and 3D DM ankle joint models were subjected to different load stress tests, with the test results shown in **Figure 6**.

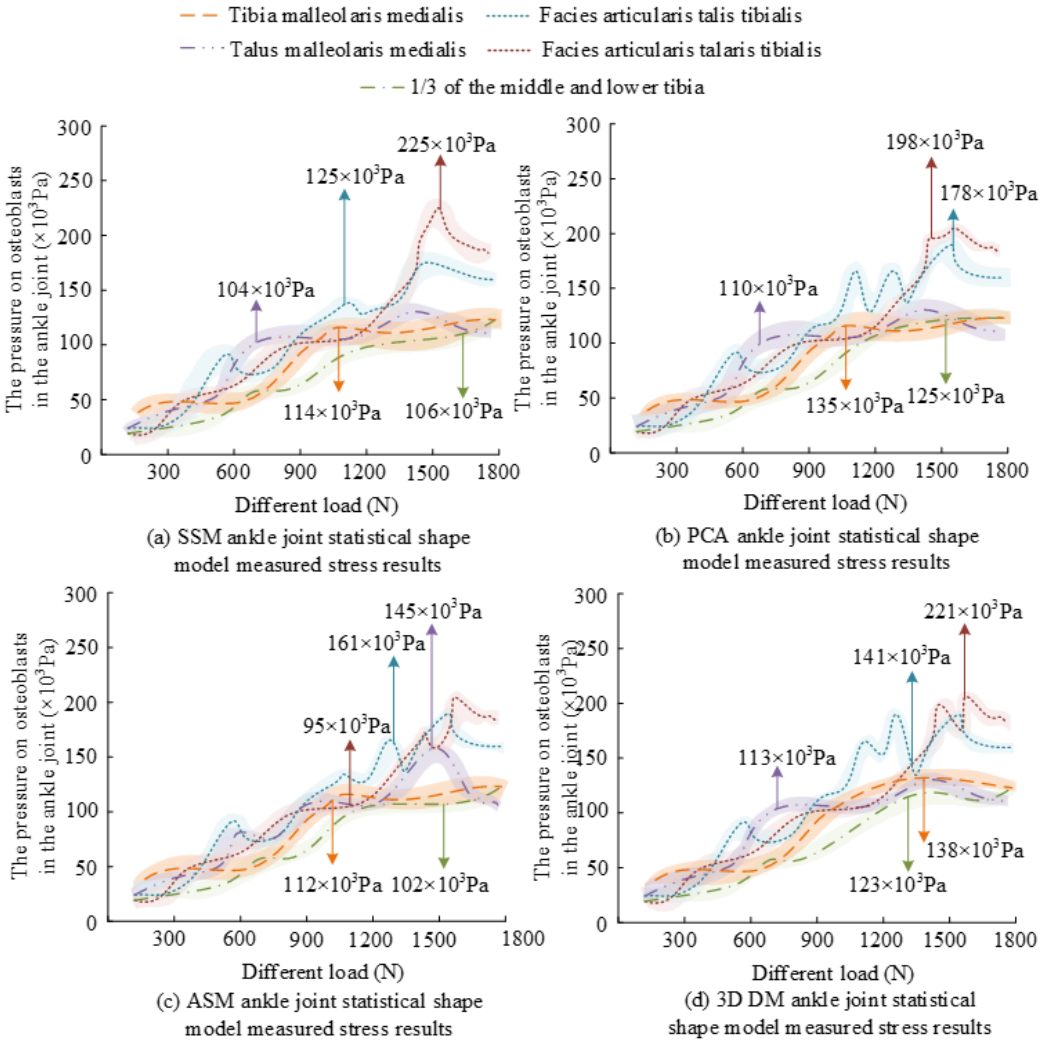

Figure 6. Stress test results of different ankle joint models.

From **Figure 6a**, it can be seen that the SSM ankle joint model exhibits the maximum displacement at the ankle joint talar head. Under a 1700 N load, the maximum stress value at the talar head reaches 225 × 10^3 Pa. From **Figure 6b**, it is observed that the PCA ankle joint model shows significant displacement changes at the tibial joint surface between 1000 N and 1500 N, with the maximum stress value reaching 178 × 10^3 Pa. From **Figure 6c**, it can be seen that the ASM ankle joint model has a maximum stress value of 145 × 10^3 Pa at the medial malleolus talus, which is lower compared to the maximum stress value of 172 × 10^3 Pa at the tibial joint surface. From **Figure 6d**, it is evident that the 3D DM ankle joint model measured higher stress values across all parts of the ankle joint, and the displacement was also more significant compared to the model proposed in this study. In addition, the research also tested the accuracy of ankle image segmentation by SSM, PCA, ASM, and 3D DM statistical shape models in the SCAPE data set and VHP data set respectively, and the test results are shown in **Figure 7**.

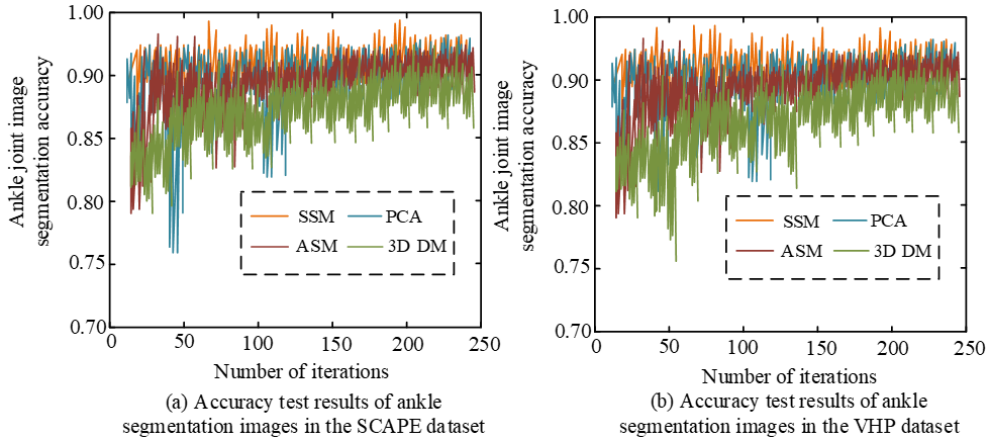

Figure 7. Image accuracy test results of ankle joint segmentation by different models in different data sets.

As can be seen from **Figure 7a**, when the SSM ankle statistical shape model has 200 iterations in the SCAPE data set, the ankle image segmentation accuracy is 0.94, and the overall image segmentation accuracy is above 0.90. As can be seen from **Figure 7b**, when the iteration times of the SSM ankle statistical shape model were 150–200 times during the test in the VHP dataset, the image segmentation accuracy was 0.92–0.98. When the iteration times of PCA and ASM statistical shape models of the ankle joint were 200 times, the image segmentation accuracy was 0.96 and 0.94, respectively. In summary, the SSM ankle joint statistical shape model also has good generalization performance in different data sets. Additionally, the study also performed tests on the SSM ankle joint model for Talus Absolute Coefficient (R^2), Mean Absolute Percentage Error (MAPE), Root Mean Square Error (RMSE), and Mean Absolute Error (MAE) accuracy indicators. The test results are shown in **Figure 8**.

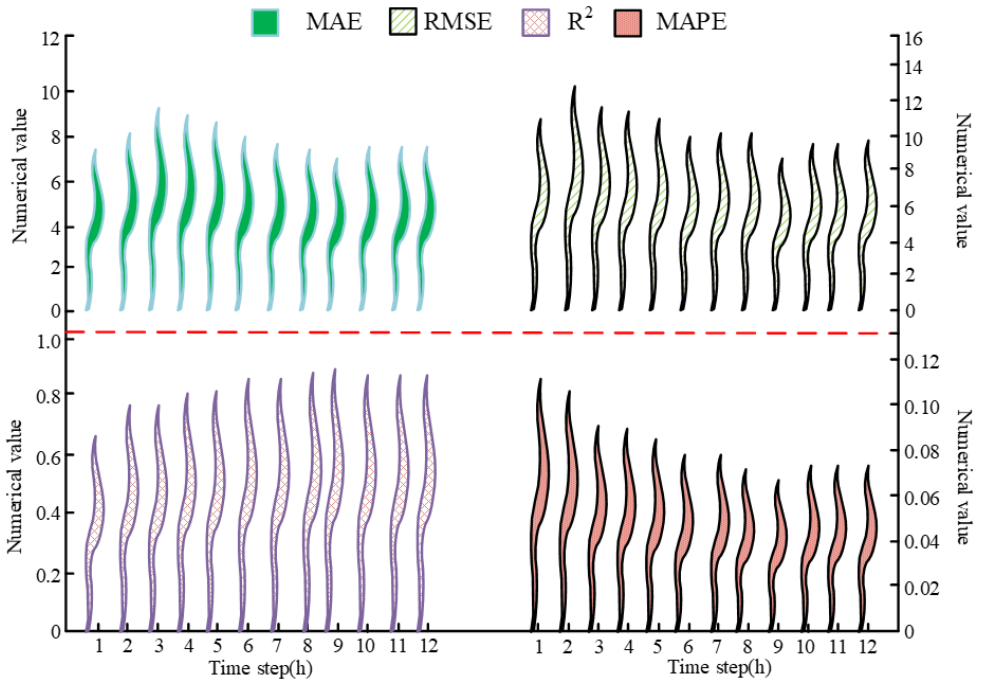

Figure 8. Test results of different indexes of SSM ankle joint model.

As shown in **Figure 8**, the red dashed line represents the boundary for the indicator tests. When the SSM ankle joint model was tested for the R^2 index of the talus, at 6 h of iteration, the R^2 index was 0.89, and it gradually approached 1.0 over time. For the MAPE test of the talus, at 1 h of iteration, the MAPE value was 0.11, and between 8 to 12 h, the MAPE value ranged from 0.06 to 0.08. In the RMSE test, the average deviation was largest at 13.14 at the 2nd hour. In the MAE test, after 5 hours of iteration, the MAE value stabilized, and at 8 h of iteration, the MAE value for the talus measurement was 7.12. To further validate the evaluation performance of the SSM ankle joint model, the study compared it with the PCA, ASM, and 3D DM ankle joint models in terms of compactness, generalization, and specificity. These three indexes were calculated by principal component analysis variance contribution rate, independent test set error and classification accuracy, with the results shown in **Figure 9**.

As shown in **Figure 9a**, in the talus compactness test, the compactness index of the SSM ankle joint model was lowest at 29,800, and when the number of variation models reached 50, the compactness index increased to 41,500. As shown in **Figure 9b**, in the talus generalization test, the SSM ankle joint model exhibited the best overall generalization performance, with the minimum generalization index reduced to 93,400, while the 3D DM ankle joint model had the lowest generalization index at 93,800. As shown in **Figure 9c**, the specificity value of the ASM ankle joint model was lowest at 92,400, while the proposed model fluctuated between 92,500 and 92,890. As shown in **Figure 9d**, in the calcaneus compactness test, the compactness index of the SSM ankle joint model increased from 116,900 to 64,700. As shown in **Figure 9e**, the PCA ankle joint model had a generalization performance second only to the SSM ankle joint model, with the SSM ankle joint model's lowest generalization index at 111,500. As shown in **Figure 9f**, the specificity index for the calcaneus in the SSM ankle joint

model fluctuated mainly between 110,200 and 110,700, showing relatively stable overall variation.

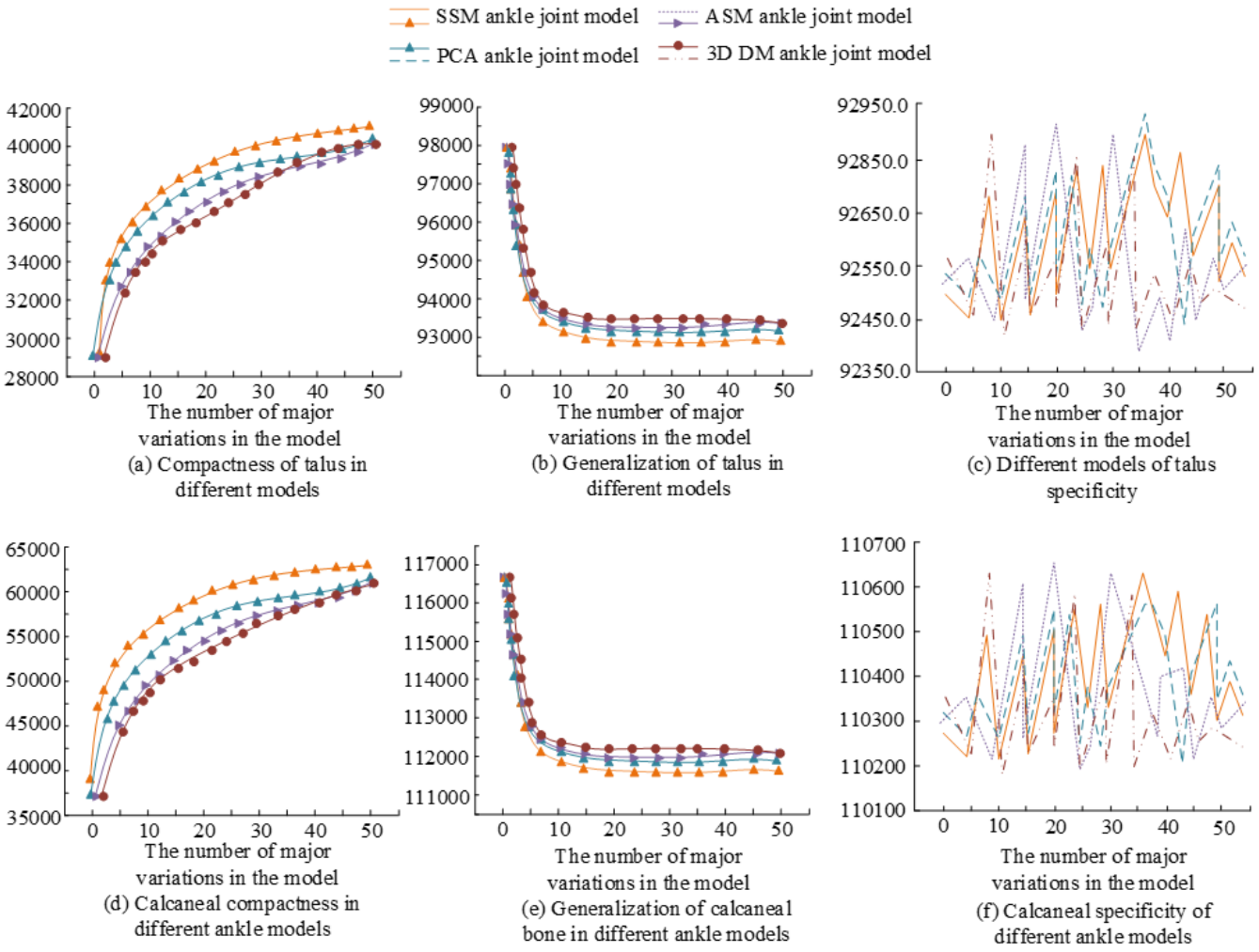

Figure 9. Compactness, generalization, and specificity test results.

3.2. Analysis of standard deviation morphology axis based on the SSM

To further verify the morphological axis space of the SSM ankle joint model, the study used Matlab software to conduct data analysis of the talus morphological axis and multiple standard deviations based on the SSM ankle joint model. The SSM-based ankle joint model mainly generated principal component models PC1–PC3, which represented the overall talus variation, talus curvature variation, and the curvature variation between the anterior joint surface and the lateral surface of the talus. In order to gain a clearer understanding of the talus, the study assessed the talus bone morphological changes by fitting the positive and negative standard deviation models of PC1–PC3 using a dual sphere fitting technique. The talus morphological axis angle changes based on the SSM model are shown in **Figure 10**.

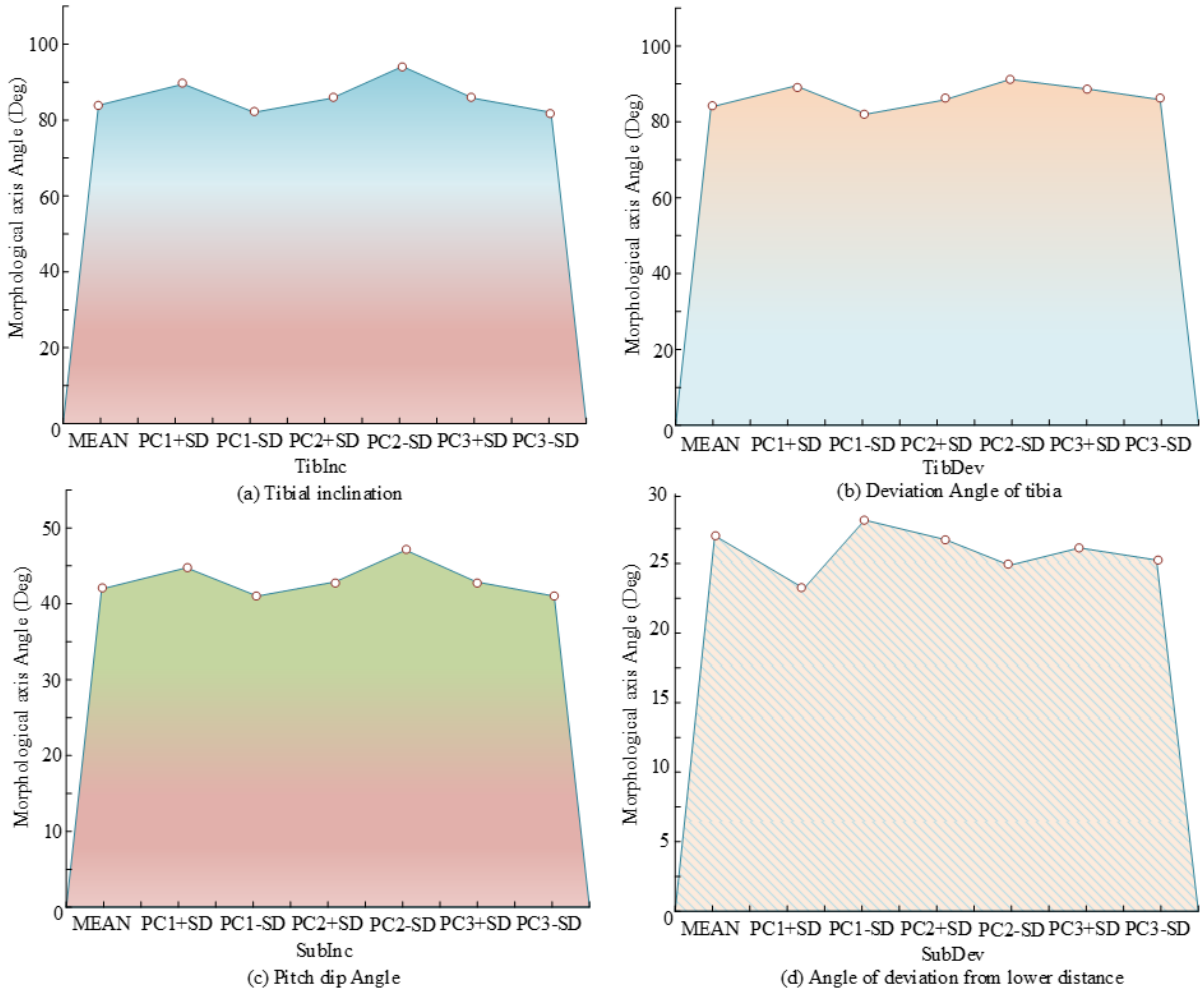

Figure 10. Morphological axis angle change map of talus based on SSM model.

As shown in **Figure 10a**, the morphological axis angle changes for PC1 + SD and PC2 − SD were quite large, with angle values of 87 and 92, respectively. The entire tibial tilt angle was most influenced by PC1 and PC2. As shown in **Figure 10b**, in the overall PC1–PC3 tibial deviation test, the overall curvature change remained relatively stable. The angle value of the PC1 − SD morphological axis was 78, which was the smallest in the talus deviation. As shown in **Figure 10c**, in the downward tilt angle test, the PC2 − SD morphological axis angle change was the greatest, with an angle value of 47. The angle changes for PC1 − SD and PC2 + SD were similar, with angle values ranging from 40 to 42. As shown in **Figure 10d**, in the downward deviation angle test, PC2 had the greatest impact on the subtalar joint axis. The angle values for the positive and negative standard deviation models of PC2 ranged from 23 to 27. Additionally, the study performed multiple standard deviation analyses on the talus morphological changes in the SSM ankle joint, with the PC1–PC3 multiple standard deviation morphological axis shown in **Figure 11**.

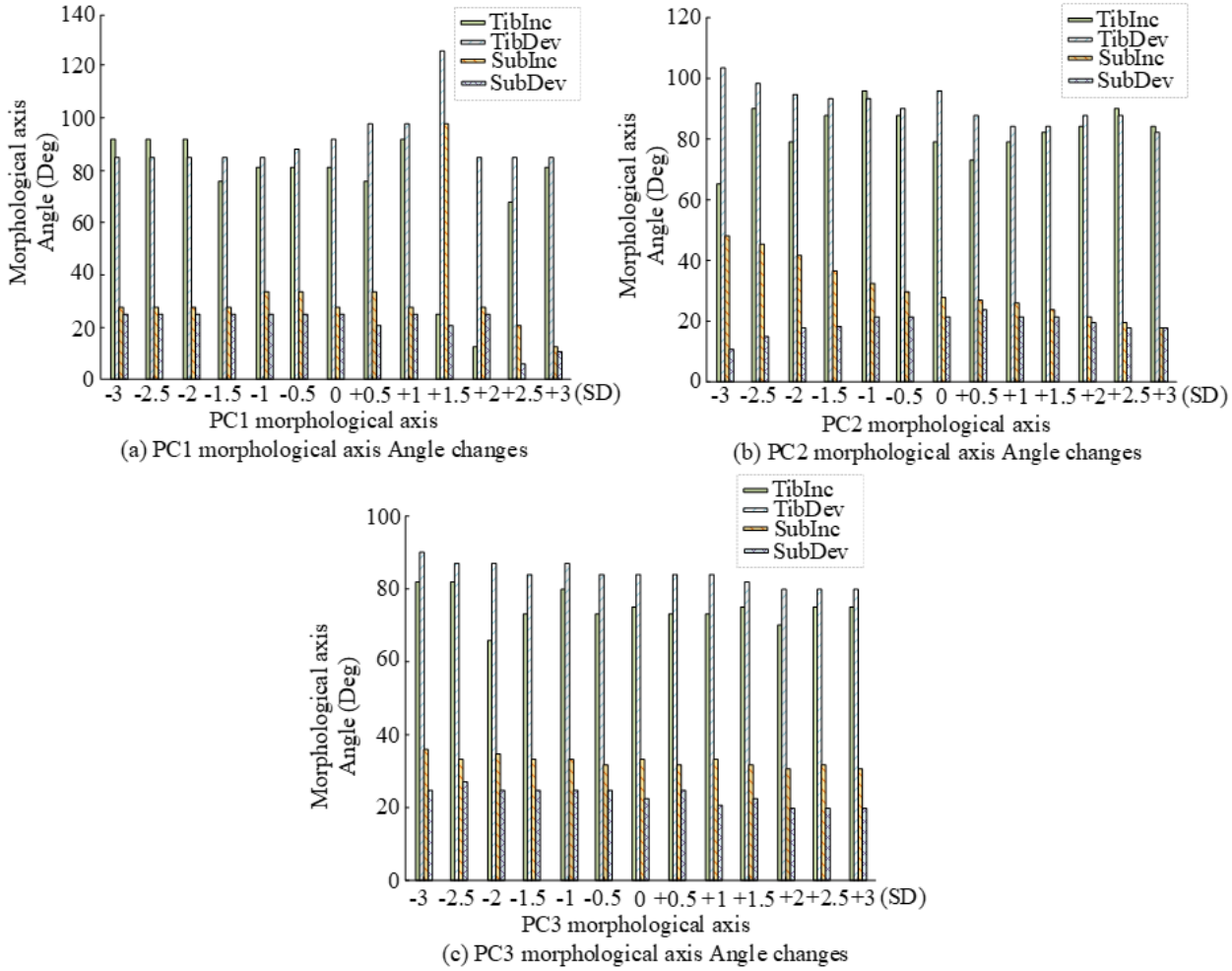

Figure 11. Multiple standard deviation analysis results.

As shown in **Figure 11a**, in the range test of PC1 ± 3 standard deviations, the tibial tilt angle results for the PC1 morphological axis showed significant differences. When the tibial deviation morphological axis was +1.5 SD, the morphological axis angle value was 124. As shown in **Figure 11b**, the talus downward tilt angle morphological axis angle value gradually decreased in the +SD direction, with the morphological axis angle value of the talus at +3 SD being 28. As shown in **Figure 11c**, the talus downward deviation angle morphological axis angle value remained relatively stable overall. The downward deviation morphological axis angle value at −3 SD was 27, while at +3 SD, the angle value was 26.

3.3. Analysis of tourist travel experience by the SSM ankle joint model

After verifying the SSM ankle model and the multi-standard deviation shape axis of the talus, in order to further demonstrate the good influence of the SSM ankle model on tourists, the study also uses the SSM ankle model to improve tourist travel equipment. In order to verify the validity of the experiment, the study tested the satisfaction of 150 tourists in Miyun ski resort. The scoring dimension of this test is mainly conducted from the two aspects of tourists' emotions and tourists' satisfaction. Tourists' satisfaction is presented in the form of a percentage. The higher the value,

the more satisfied they are with the tourism equipment. And the test results are shown in **Table 2**.

Table 2. Visitor satisfaction test results.

Ski equipment	Tourist mood	Tourist satisfaction/%
Veneer	Be delighted	95
Double plate	Irritate	89
Snowshoe	Enjoy	95
Skis	Secure	97
Skateboard	Excitement	96
Ski	Be delighted	96
Ski suit	Be delighted	99

As can be seen from **Table 2**, the improved equipment with the highest tourist satisfaction is ski clothing, with a travel satisfaction of 99%. When tourists experience skiing, the lowest satisfaction is double-board equipment. Because the double board is suitable for more advanced skiing, the skiing mood of tourists is more exciting and nervous, and the tourism satisfaction rate is 89%. The overall satisfaction of the improved skiing equipment based on SSM is more than 85%, and tourists are greatly satisfied with the improved physical and mental experience of skiing equipment and pay more attention to tourism experience in skiing.

4. Discussion

The proposed SSM-based ankle joint model demonstrated significant advantages in the performance comparison experiments. From multiple perspectives, including load stress variation, mean absolute percentage error, three-dimensional model compactness, and generalization, the SSM ankle joint model outperformed the PCA, ASM, and 3D DM ankle joint models. Specifically, in the load stress tests, the SSM ankle joint model measured a stress of 225×10^3 Pa at a 1700 N load on the talus. This model was able to store the talus displacement data and provide timely feedback to the motion tester, primarily due to the improved data collection system and three-dimensional modeling capabilities. This result was similar to the conclusions found by Huang et al. in their 2024 study [19]. Furthermore, in the accuracy mean absolute error test, the SSM-based ankle joint model also provided good predictions for different ankle joint data. The talus measurement showed an MAE value of 7.12 after 8 h of iteration, and the MAPE value ranged from 0.06 to 0.08 during the 8–12 h period. The SSM ankle joint model also performed excellently in the compactness, generalization, and specificity tests. The compactness index of the SSM ankle joint model reached 41,500 when the number of variant models reached 50, whereas the compactness indices of the PCA, ASM, and 3D DM models were all lower than the proposed model. This can mainly be attributed to the SSM model's integration of three-dimensional reverse modeling and optical motion capture systems during data collection. In addition, in order to better capture the local nonlinear features of the ankle shape, the SSM model also introduced local linear embedding to carry out point linear reconstruction of the local domain and mapped the calculated local linear

reconstruction coefficient to the low-dimensional space during the point linear reconstruction, so that the data structure of the SSM model in the low-dimensional space was easier to understand and analyze. These findings were consistent with the results obtained by Burton et al. when testing ankle joint models [20].

When the SSM ankle joint model was further analyzed through multiple standard deviation morphological axis experiments for the talus, it also demonstrated superior performance. In tests of the tibial tilt angle and tibial deviation angle, the measurements of PC1–PC3 talus data showed that the greatest changes in morphological axis angles occurred at PC1 + SD and PC2 − SD, with angle values of 87 and 92, respectively, while the downward deviation angle value was 26.02. In addition, the improvement of the ski equipment based on the SSM ankle joint model also brings a good sense of experience to the tourists, among which the experience satisfaction of snowboarding is 95%. In the range test of PC1 ± 3 standard deviations, the tibial deviation morphological axis at +1.5 SD yielded a morphological axis angle value of 124. In summary, the SSM-based ankle joint model is capable of recognizing variations in the talus range and analyzing the stress on the talus in detail. Therefore, the ankle joint model based on SSM can be intelligently designed for ski sports equipment, and in the future, custom equipment can be produced by 3D printing, and its biomechanical properties can be tested to improve the related travel experience.

The contributions of the study are mainly reflected in the following two aspects: first, a data collection method combining optical motion capture systems and three-dimensional reverse modeling was designed; second, an SSM ankle joint model was proposed based on the improved data collection method, providing a new research approach for skiing biomechanics.

5. Conclusion

In response to the challenges of ankle joint skeletal data collection in skiing biomechanics, the study proposed an SSM-based ankle joint model that establishes relevant connections between ankle joint morphology and the talus. The model integrates the use of an optical motion capture system for ankle joint data collection and three-dimensional reverse modeling for visual effect demonstration. To ensure the accuracy of the ankle joint mechanical data, an error correction algorithm was applied to correct axial force data. The experimental results show that the ankle joint model based on SSM can perform well on the key indicators of ankle joint compactness, generalization, and specificity, and the accuracy and efficiency are up to high standards. The improved ski equipment based on SSM also gives tourists a good satisfaction experience. At present, the experiment has not conducted relevant tests on human gait in skiing sports, and the research still has shortcomings in feature sequence extraction and foot bone structure surface tests, etc. It is necessary to further expand the sample size and expand the experimental group. Further tests could be carried out in the future in areas such as clinical medicine or biomechanics of the ankle under fatigue conditions.

Author contributions: Conceptualization, NL and RF; methodology, RF; software, TF; data curation, RF; writing—original draft preparation, NL; writing—review and

editing, TF; visualization, RF. All authors have read and agreed to the published version of the manuscript.

Ethical approval: Not applicable.

Conflict of interest: The authors declare no conflict of interest.

References

1. Cao Y, He J, Chen X, et al. The impact of ankle movements on venous return flow: A comparative study. Phlebology: The Journal of Venous Disease. 2024; 39(10): 676-682. doi: 10.1177/02683555241264914
2. Toda H, Kawamoto H. Device Design of Ankle Joint Stretching System Controlled by the Healthy Side Ankle Joint Movement for Self-Rehabilitation. Journal of Robotics and Mechatronics. 2023; 35(3): 556-564. doi: 10.20965/jrm.2023.p0556
3. Shi X, Cao Z, Ganderton C, et al. Ankle proprioception in table tennis players: Expertise and sport-specific dual task effects. Journal of Science and Medicine in Sport. 2023; 26(8): 429-433. doi: 10.1016/j.jsams.2023.06.010
4. Reynolds RF, Liedtke AM, Lakie M. Intrinsic ankle stiffness is associated with paradoxical calf muscle movement but not postural sway or age. Experimental Physiology. 2024; 109(5): 729-737. doi: 10.1113/ep091660
5. Li Y, Wang Z, Shen Y, et al. Differences in Cortical Activation During Dorsiflexion and Plantarflexion in Chronic Ankle Instability: A Task-fMRI Study. Clinical Orthopaedics & Related Research. 2023; 482(5): 814-826. doi: 10.1097/corr.0000000000002903
6. Han S, Lee H, Son SJ, et al. Effect of varied dorsiflexion range of motion on landing biomechanics in chronic ankle instability. Scandinavian Journal of Medicine & Science in Sports. 2023; 33(7): 1125-1134. doi: 10.1111/sms.14339
7. Liu T, Dimitrov A, Jomha N, et al. Development and validation of a novel ankle joint musculoskeletal model. Medical & Biological Engineering & Computing. 2024; 62(5): 1395-1407. doi: 10.1007/s11517-023-03010-x
8. Cai X, Wu Y, Huang J, et al. Application of statistical shape models in orthopedics: a narrative review. Intelligent Medicine. 2024; 4(4): 249-255. doi: 10.1016/j.imed.2024.05.001
9. Trentadue TP, Thoreson A, Lopez C, et al. Morphology of the scaphotrapeziotrapezoid joint: A multi-domain statistical shape modeling approach. Journal of Orthopaedic Research. 2024; 42(11): 2562-2574. doi: 10.1002/jor.25918
10. Chollet M, Hintzy F, Cross MR, et al. Fatigue-induced alterations in force production, trajectory and performance in alpine skiing. Journal of Sports Sciences. 2024; 42(20): 1904-1915. doi: 10.1080/02640414.2024.2414362
11. Nguyen TT, Nguyen QD, Ha MQ, et al. The Development of a Motion-Tracking System to Assess the Recovery Level for Stroke Survivors. Acta Polytechnica Hungarica. 2024; 21(9): 9-28. doi: 10.12700/aph.21.9.2024.9.2
12. Romero-Flores CF, Bustamante-Bello R, Moya Bencomo M, et al. Optical Marker-Based Motion Capture of the Human Spine: A Scoping Review of Study Design and Outcomes. Annals of Biomedical Engineering. 2024; 52(9): 2373-2387. doi: 10.1007/s10439-024-03567-0
13. Lugrís U, Pérez-Soto M, Michaud F, et al. Human motion capture, reconstruction, and musculoskeletal analysis in real time. Multibody System Dynamics. 2023; 60(1): 3-25. doi: 10.1007/s11044-023-09938-0
14. Sakai R, Kenmoku T, Tazawa R, et al. Stresses in the Scapular Fossa Do Not Exceed the Yield Stress When Elevated up to 135 Degrees of Abduction after Reverse Shoulder Arthroplasty. Journal of Biomedical Science and Engineering. 2024; 17(02): 35-40. doi: 10.4236/jbise.2024.172003
15. Kolac UC, Paksoy A, Akgün D. Three-dimensional planning, navigation, patient-specific instrumentation and mixed reality in shoulder arthroplasty: a digital orthopedic renaissance. EFORT Open Reviews. 2024; 9(6): 517-527. doi: 10.1530/eor-23-0200
16. Anderson DD, Ledoux WR, Lenz AL, et al. Ankle osteoarthritis: Toward new understanding and opportunities for prevention and intervention. Journal of Orthopaedic Research. 2024; 42(12): 2613-2622. doi: 10.1002/jor.25973
17. Daneshvarhashjin N, Debeer P, Innocenti B, et al. Covariations between scapular shape and bone density in B-glenoids: A statistical shape and density modeling-approach. Journal of Orthopaedic Research. 2023; 42(5): 923-933. doi: 10.1002/jor.25747
18. Tran VD, Vo PP, Tran NLN, et al. A statistical shape modelling method for predicting the human head from the face. International Journal of Biomedical Engineering and Technology. 2024; 46(1): 1-26. doi: 10.1504/ijbet.2024.140689

19. Huang M, Yu B, Li Y, et al. Biomechanics of calcaneus impacted by talus: a dynamic finite element analysis. Computer Methods in Biomechanics and Biomedical Engineering. 2023; 27(7): 897-904. doi: 10.1080/10255842.2023.2213369
20. Burton W, Myers C, Stefanovic M, et al. Scan-Free and Fully Automatic Tracking of Native Knee Anatomy from Dynamic Stereo-Radiography with Statistical Shape and Intensity Models. Annals of Biomedical Engineering. 2024; 52(6): 1591-1603. doi: 10.1007/s10439-024-03473-5